ELSEVIER

Journal of Nuclear Materials 313–316 (2003) 787–795

journal of nuclear materials

www.elsevier.com/locate/jnucmat

Narrow power profiles seen at JET and their relation to ion orbit losses

W. Fundamenski [a,*], S. Sipilä [b], T. Eich [a], T. Kiviniemi [b], T. Kurki-Suonio [b], G. Matthews [a], V. Riccardo [a], Contributors to the EFDA-JET work programme

[a] *Euratom/UKAEA Fusion Association, Culham Science Centre, Abingdon, Oxon, UK*

[b] *Tekes-Euratom Association, Helsinki University of Technology, P.O. Box 2200, HUT FIN-02015, Finland*

Received 27 May 2002; accepted 12 September 2002

Abstract

Recent JET measurements of heat load profiles during NBI-heated, natural density, ELMy H-modes revealed highly peaked profiles. In this study, ion orbit loss (IOL) from the core periphery was simulated numerically on four selected JET discharges (two high power H-modes, a fuelled H-mode and an L-mode), using realistic magnetic geometry and 2-D plasma/neutral background. The simulated and measured profiles agree quite well in all discharges, suggesting that IOL is indeed the mechanism responsible for the narrow profiles. The interaction between energetic ions and scrape-off layer (SOL) ions/atoms was also investigated, resulting in SOL power stopping factors of 60–80%. The momentum transfer via IOL to background ions was found to be in the same direction as the observed SOL flows (towards the inner target) but too small to be their primary cause. Preliminary simulation of IOL on ITER indicate peak heat loads <2 MW/m^2 at the outer target.

PACS: 52.40.H

Keywords: Divertor; Boundary plasma; Power handling; SOL; Edge modelling

1. Introduction

Power handling remains one of the key constraints on ITER divertor design. Recent JET results using the thermocouple (TC) technique reveal highly peaked outer target power deposition profiles during high power, unfuelled, ELMy H-modes [1,2]. Combining the above results with Langmuir probe (LP) measurements of electron power, suggests that energetic ions are responsible for the narrow profiles [3]. This suggestion was initially put forth based on preliminary fluid modelling of the scrape-off layer (SOL) plasma, which indicated collisionless conditions for separatrix ions [4]. In subsequent analysis, ion orbit loss (IOL) from the edge transport barrier (ETB) region emerged as the most likely explanation for the observed narrow profiles [3]. The aim of the present paper was to simulate IOL on JET numerically, allowing a quantitative comparison with experiment.

The paper is organized as follows: Section 2 describes the diagnostics and experimental data available from JET to date; Section 3 discusses the edge plasma/neutral reconstructions using the OSM2/EIRENE code package; Section 4 presents the results of the kinetic modelling of IOL effects in JET using the ASCOT code; finally Section 5 draws conclusions and outlines future work.

2. Measurements of power deposition on JET

2.1. Divertor diagnostics

There are three diagnostic systems available on JET for measuring power deposition profiles on the MkIIGB

* Corresponding author. Tel.: +44-1235 464946; fax: +44-1235 464882.

E-mail address: wfund@jet.uk (W. Fundamenski).

0022-3115/03/$ - see front matter
PII: S0022-3115(02)01432-0

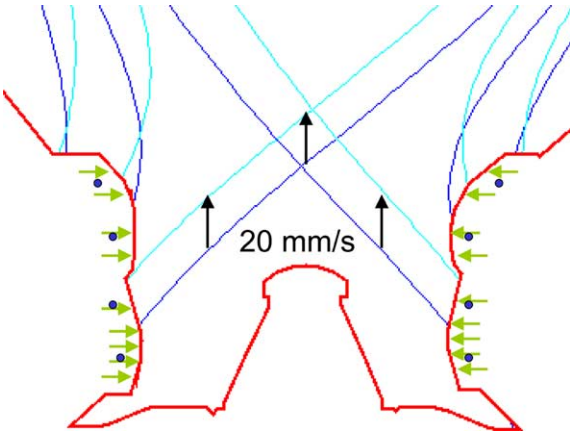

Fig. 1. Poloidal cross-section of the MkIIGB divertor showing the location of TCs (circles), LPs (arrows) and infra-red thermography; the IR camera has a good view of both the inner and outer vertical targets.

divertor tiles. These are the TC technique, LP and infra-red thermography (IR). The position of these diagnostics in the JET MkIIGB divertor is shown in Fig. 1, along with a typical equilibrium used for profile measurement.

The TC technique consists of shifting the strike point vertically during the flat top phase of the discharge and reconstructing the power profile using finite element modelling of the vertical divertor tile [2]. The vertical shift is slow enough (~20 mm/s) that an e-folding length encompasses many (>10) ELM events. As such, the TC method provides total, ELM-averaged power profiles, $q_{\mathrm{tot}}(r)$. It is the primary diagnostic used in this study.

The MkIIGB divertor is equipped with an array of LPs [5]. These measure the plasma flux Γ_0, electron temperature T_e, and the parallel electron power flux $q_{\|e} \sim 5T_e\Gamma_0$ leaving the plasma. By using a vertically shifted discharge, an electron power profile can be obtained from a single probe. For the purposes of comparison, the probe closest to the TC position on the vertical target was chosen, which allowed for a direct comparison of the total and electron power profiles. Although LP's register ELM events, they do not provide accurate information about ELM power, even in the electron channel. Therefore, LP profiles correspond to the inter-ELM electron power flux, $q_e(r)$.

Infra-red thermography is the most common, and until recently the only, technique used for measuring total power deposition profiles. For example, the ITER divertor has been designed based exclusively on IR power width measurements on three machines (D-IIID, AUG, JT-60). On JET the IR system operates close to its spatial resolution limit (only few pixels per profile width), which complicates the interpretation of photon flux data. This was one of the reasons cited for a discrepency between TC and IR profiles on JET in the past [3]. During the 2001 shutdown, an in-vessel calibration of the system was performed which allowed the instrument function of the IR camera to be calculated. Using this function, the IR photon fluxes were deconvoluted, leading to more accurate power flux profiles. The resulting IR profiles are compared with both TC and LP profiles for two typical shots: 3.3 MW L-mode and 16 MW unfuelled H-mode, Fig. 2. For both shots the IR and TC profiles agree quite well, both in the peak heat flux and in the full-widths at half-maximum (FWHM), which are also well matched by LP widths. The lower magnitude of the LP profile in the H-mode case, implies a dominant ion contribution to the total deposited power (contributions from radiation and CX neutrals have been estimated as two orders of magnitude below the peak TC value [3]). Most notably for ITER, all three diagnostics indicate a reduction in profile width (FWHM) with input power, in contrast to the ITER-99 database [6].

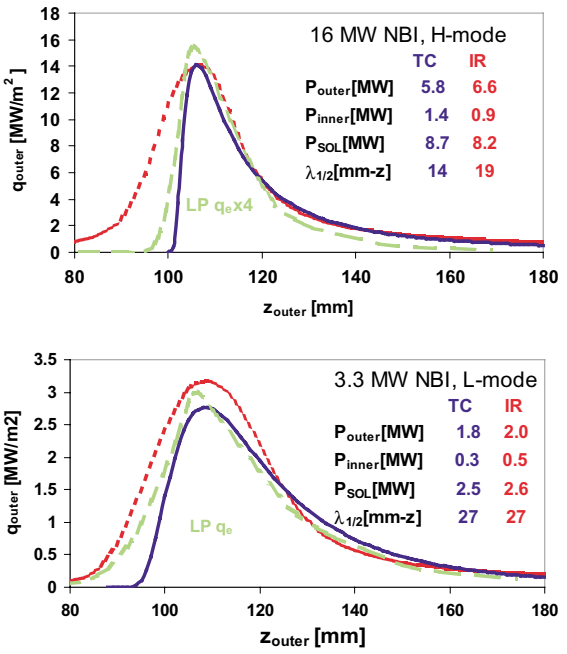

Fig. 2. Radial profiles of heat load on the outer target, as calculated by TC (solid), IR (dashed) and LP (grey dashed) diagnostics for two JET discharges. In the H-mode case, the LP profile has been multiplied by four to show the similarity in shape to the TC profile.

2.2. Deuterium plasmas

In pure deuterium plasmas, power deposition profiles were measured using the TC and LP methods in a series of identical 2.5 MA/2.4 T discharges involving a scan in the NBI heating power (4–16 MW, where $P_{\mathrm{L\text{-}H}} \sim 5$ MW)

and a D_2 fuelling rate ($0–3 \times 10^{22}$ s^{-1}; $f_{GW} \sim 0.65–0.9$). Since peak heat fluxes were much larger at the outer than the inner targets (factor of five or more), the following discussion is restricted exclusively to outer target data. Regression analysis lead to the following expression for the integral power width λ_q^{int} at the outer target,

$$\lambda^{int}_{q\,\text{JET-}TC\text{-}D} \sim P^{-0.45\pm0.1}_{target} n^{0.40\pm0.1}_{sep}, \quad (1)$$

where P_{target} is the power reaching the outer target and n_{sep} is the upstream separatrix density [3]. In terms of magnitude, λ_q^{int} varried by a factor of two from ~7 mm-omp (mapped to the outer mid-plane) in L-mode and high-fuelled H-mode to 3.5 mm-omp at the natural density and highest power. The inverse power scaling in the above expression stands in sharp contrast to the ITER-99 database,

$$\lambda^{int}_{q\,\text{ITER-99-D}} \sim P^{+0.35\pm0.1}_{target}, \quad (2)$$

where a positive power scaling is indicated [6]. The positive density dependence reflects the suppression of the narrow feature by additional gas fuelling. The ion peak heat flux was obtained by subtracting the TC (total) and LP (electron) peak heat fluxes, $q_i = q_{tot} - q_e$. It was found that ions dominate the total peak heat flux in the presence of narrow power profiles, e.g. in unfuelled, high power H-modes, while electrons dominate in L-mode and fuelled H-modes. The strong correlation between the high ion fractions and profile peaking suggests that energetic ions are responsible for this phenomenon. The estimated temperature of these ions ($T_i \sim q_i / 2.5\Gamma_0 \sim 250$ eV) places their origin in the ETB region, between the top of the pedestal ($T_e^{ped} \sim 1$ keV) and the separatrix ($T_e^{sep} \sim 100$ eV). This does not rule out a possible contribution from beam ions or fusion alpha's (detailed kinetic calculations of these effects are underway) but it suggests that their contribution is secondary to the thermal pedestal ions.

2.3. Helium plasmas

In the 2001 experimental campaign, similar measurements were repeated in pure He plasmas [7]. Additional variation in toroidal field B_t, magnetic safety factor q_{95} and ion charge(mass) Z(A) included in these experiments allowed the scaling (1) to be extended to included these parameters. Regression analysis of the combined set of D and He discharges lead to the following expression for the integral power width at the outer target [8],

$$\lambda^{int}_{q\,\text{JET-TC-D/He}} \propto Z^{0.85\pm0.1} B_t^{-1.1\pm0.3} q_{95}^{0.65\pm0.1} P^{-0.3\pm0.1}_{target}. \quad (3)$$

The relatively small error bars seen in the exponents indicate good quality of the resulting fit. Since no statistically meaningful density dependence was observed, it was not included in the final scaling. Following the method of Connor et al. [9], the above expression for λ_q has been compared with the predictions of roughly two dozen candidate theoretical models for radial heat diffusivity $\chi_\perp$ in the SOL. The best fit to the experimental data was obtained using the classical model for $\chi_\perp$, with the neo-classical estimate a distant second [8]. This finding further confirmed the hypothesis that IOLs are responsible for the narrow power profiles, since IOL combines elements of classical and neo-classical transport. The remainder of the paper will attempt to assess this hypothesis based on numerical modelling of IOL in selected JET discharges.

3. Edge plasma/neutral modelling

The algorithm used to model IOL in the present study is summarized below,

Equilibrium (EFIT)
↓
Numerical Mesh (GRID2D)
↓
2D Edge plasma/neutral background (OSM2/EIRENE)
↓
3D Monte-Carlo IOL (ASCOT)

The numerical mesh was first constructed based on EFIT data for the appropriate time slice of a selected discharge using the GRID2D mesh generator [10]. The edge plasma/neutral background was then reconstructed using the OSM2/EIRENE code package on the previously generated grids. OSM2 is an onion-skin solver (in which radial information is introduced directly from target LP profiles) for plasma transport equations in the fluid (Braginskii) approximation, with separate equations for ion and electron energies [11]. EIRENE is a Monte-Carlo neutral hydrogen transport code [12]. The two codes are coupled and iterated until mutual convergence. In all cases, it was assumed that equal power enters the ion and electron channels, a conservative assumption which underestimates the power to the ions. The above procedure was performed for four identical JET discharges (2.5 MA/2.4 T, $q_{95} = 2.6$): two unfuelled H-modes at different power levels, 50 401 (12 MW, $f_{GW} \sim 0.65$) and 50 421 (16 MW, $f_{GW} \sim 0.65$), a strongly fuelled H-mode 50 404 (12 MW, $f_{GW} \sim 0.9$) and one L-mode discharge at much lower power, 50 414 (3.3 MW, $f_{GW} \sim 0.3$). The above four shots effectively map out the boundaries of the power and density scan experiments discussed in Section 2.2. In order to form a composite picture of the edge plasma, diagnostic radial profiles of density and temperature were used inside of the separatrix (LIDAR for n_e, ECE for T_e, with $T_i = T_e$ assumed,

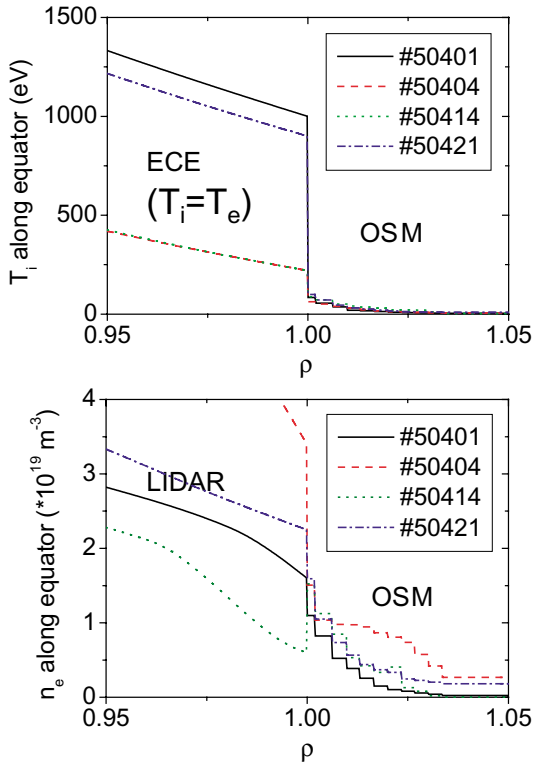

Fig. 3. Composite profiles of ion temperature and density at the outer mid-plane for four selected JET discharges, plotted vs. the flux radius, with separatrix at $\rho = 1.0$. For $\rho < 1.0$, n_e was obtained from core LIDAR, while T_i from ECE T_e measurement (assuming $T_i = T_e$). For $\rho > 1.0$, n_e and T_e were obtained from OSM2/EIRENE reconstructions.

Table 1
Key parameters of four JET discharges selected for detailed OSM2/EIRENE-ASCOT modelling

	50 401	50 404	50 414	50 421
P_{NBI} (MW)	12	12	4	16
Γ_D (10^{22} s^{-1})	0	3.0	1.5	0
H/L, f_{ELM} (Hz)	H,10	H,35	L	H,15
P_{SOL} (MW)	7.2	5.6	2.5	9.0
P^{TC} (MW)	4.8	3.2	1.8	6.5
P^{LP} (MW)	1.6	2.2	1.9	2.8
q_{TC}^{peak} (MW/m^2)	10.8	5.2	2.7	17.2
q_{LP}^{peak} (MW/m^2)	4.3	5.3	2.8	5.0
q_i^{peak} (MW/m^2)	6.5	~0	~0	12.2
$q_i^{peak}/q_{tot}^{peak}$ (%)	60	<10	<10	70
λ_q^{int} (mm-omp)	4.0	7.5	7.1	3.4
$\nu_{ii,ped}$ (m)	0.05	1.1	0.7	0.07
$\nu_{ii,sep}$ (m)	1.5	4.2	3.6	1.45
$3T_{e,t}/\lambda_q^{int}$ (V/mm)	18	3.5	6.8	31

All deposited powers, heat loads and widths refer to the outer target.

as suggested by CX measurements). The composite radial profiles at the outer mid-plane for the four JET shots are plotted in Fig. 3, with key parameters summarized in Table 1. In unfuelled H-modes ions dominate the peak target heat load, $q_i/q_{tot} > 0.6$, while in the fuelled H-mode and L-mode plasmas, they play a secondary role, $q_i/q_{tot} < 0.2$. This results is consistent with the pedestal and separatrix values of ion collisionalities, which indicate ion–ion mean-free-paths comparable to the connection length to the target in the unfuelled H-mode plasmas (this is a necessary condition for the existence of direct IOL to the divertor targets). However, the key test of the IOL hypothesis consists in its ability/inability to capture the above difference in ion power fractions (q_i/q_{tot}) and quantitatively replicate the observed profiles (peak heat flux, integral width). This point will be addressed in the following section which deals with numerical modelling of IOLs.

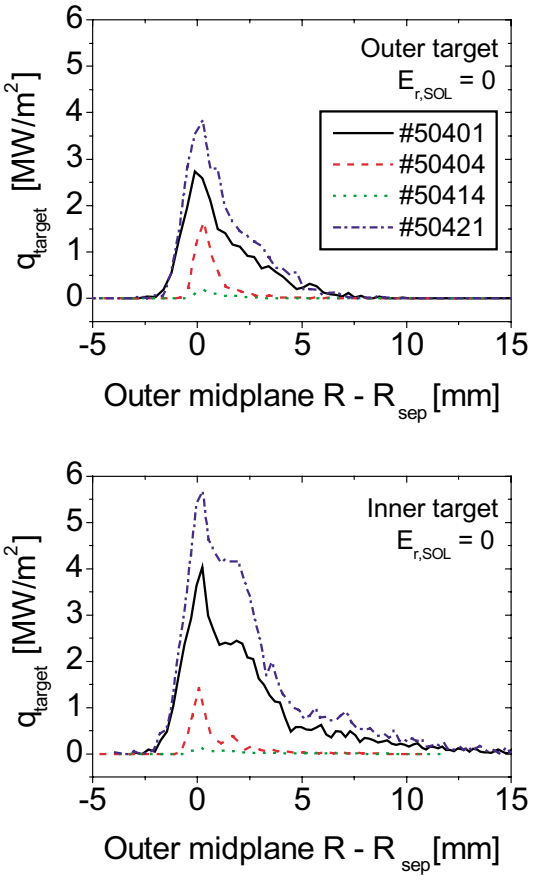

Fig. 4. Simulated heat load profiles at the outer and inner targets for with $E_{r,SOL} = 0$ for four selected JET discharges.

4. IOL modelling

4.1. ASCOT description

IOL was modelled for the four discharges of Table 1 using the ASCOT code (accelerated simulation of charged particle orbits in a Tokamak) [13]. ASCOT is a 3-D, Monte-Carlo code which follows ion orbits in the guiding centre approximation, taking account of collisions with the plasma/neutral background obtained in the previous section. The ions are launched based on core profiles of density and temperature, and followed until they either diffuse inwards into the core or outwards into the SOL and terminate by striking one of the divertor targets. Collisions with background ions and neutrals are recorded to produce a 2-D map of energy and momentum transfer. The radial electric field in the core $E_{r,core}$ is calculated self-consistently by ASCOT, but the SOL field $E_{r,SOL}$ is not computed. Previous work revealed that the IOL asymmetry is strongly dependent on $E_{r,SOL}$ due to the $\mathbf{E} \times \mathbf{B}$ drift in the SOL [3]. For this reason, all simulations were performed at four $E_{r,SOL}$ values which span the range of estimated SOL fields in the modelled discharges (no direct measurement of this quantity is available at the moment).

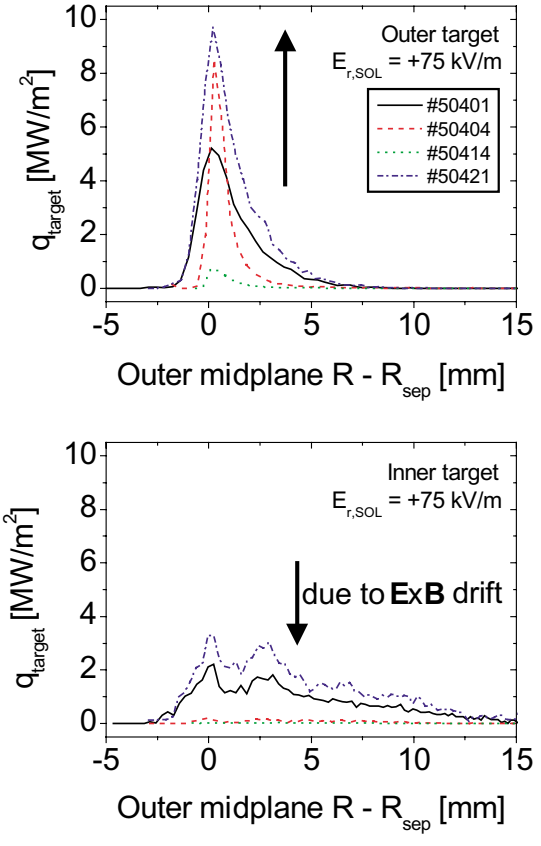

Fig. 5. Same as Fig. 4, expect with $E_{r,SOL} = 75$ V/mm-omp. The inner target profiles are reduced and broadened due to the $E \times B$ drift.

4.2. Target loads due to IOL

Using ASCOT, the ion power deposition profiles on each target were calculated for the four selected discharges and four values of radial electric field in the SOL. Theses are shown in Figs. 4 and 5 for two limiting field values (0 and +75 V/mm-omp). The null field results, Fig. 4, allow us to draw several conclusions:

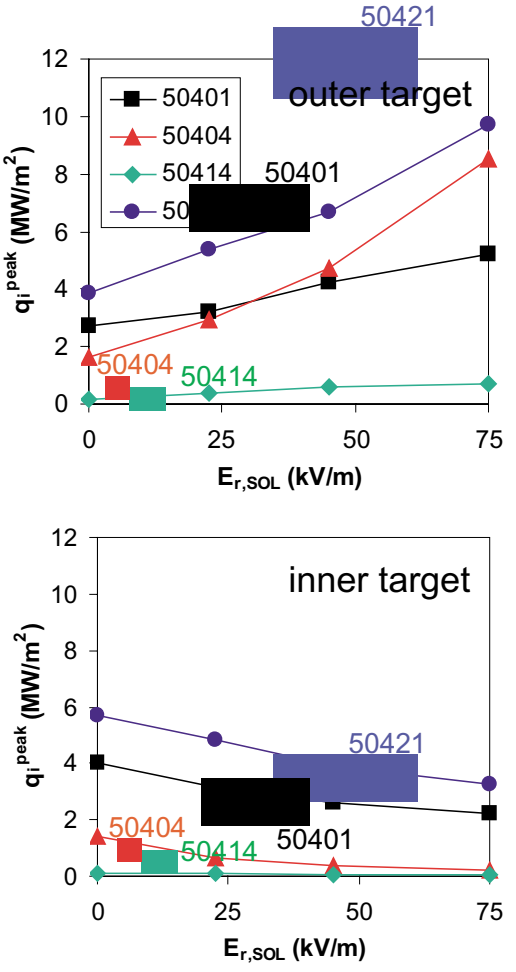

Fig. 6. Comparison of simulated and measured peak heat loads for four selected JET discharges. Shaded regions represent the experiment, taking account of the error bars in TC/LP values and in the estimates of the radial electric field in the SOL ($E_{r,SOL} > 3\ \nabla_\perp\ T_e$).

- In the absence of a pedestal, i.e. in L-mode, the IOL target load is negligible (50 414).
- In H-mode, IOL is strongly reduced by additional fuelling; suppression is more pronounced at the inner target (50 401 and 50 404).
- In unfuelled H-modes, IOL target load increases with input power with typical values of peak heat loads of several MW/m^2 (50 401 and 50 421).
- Profile FWHM widths are in the range of 2–5 mm-omp; for comparison, the D^+ gyro-radius at 1.9 T (B_t value at omp when $B_t = 2.4$ T on axis) is 2.35 mm at 1 keV and 0.74 mm at 100 eV; the poloidal gyro-radius is typically a factor $B_t/B_p \sim q_{95}(R/a) \sim$ 10 times larger.
- IOL is fairly symmetrical, with somewhat more loss to the inner target.

All, but the last, of the above points agree with experiment. Examining the high-field case (+75 V/mm-omp), Fig. 5, we see that the positive electric field increases the outer heat load with no effect on profile width, while decreasing the inner heat load and broadening the inner profiles. The net in:out asymmetry increases in favour of the outer target to the range of experimental values, typically ~1:5.

A detailed quantitative comparison requires an estimate of the SOL electric field for the four discharges of Table 1. A simple estimate of $E_{r,SOL}$ may be obtained using the electrostatic sheath expression [14], where $T_{e,t}$ is the target electron temperature,

$$E_{r,SOL} \sim 3\nabla_{\perp} T_e \sim 3T_{e,t}/\lambda_{T_e}. \quad (4)$$

Based on this estimate, $E_{r,SOL}$ is much larger in unfuelled H-mode, where electrons are hotter and profiles thinner than in fuelled H-mode or L-mode plasmas, see Table 1. The above method is fairly crude as it ignores potential drop in the pre-sheath ($<0.5T_{e,u}$ where $T_{e,u}$ is the upstream electron temperature), and finite Larmor radius effects, which could increase the magnitude of $E_{r,SOL}$ beyond a factor of two. However, it has the virtue of simplicity and should at the very least capture the scaling of $E_{r,SOL}$ with T_e and λ_{SOL}.

A comparison of the ASCOT results with experiment is shown in Fig. 6, where the peak IOL heat flux is plotted vs. $E_{r,SOL}$ for both targets and four selected discharges. The shaded regions correspond to the experi-

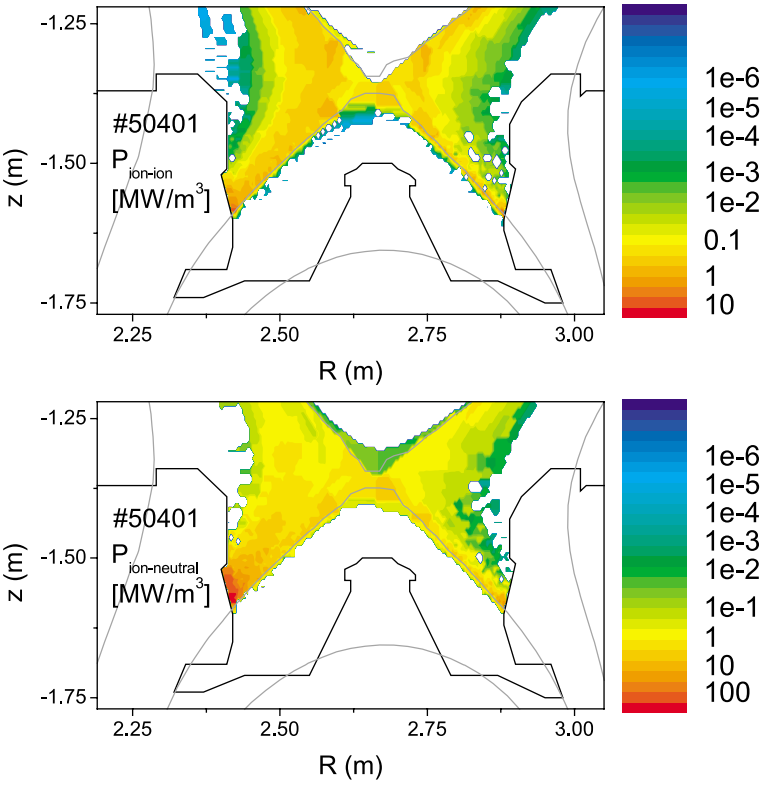

Fig. 7. Poloidal distribution of energy densities created in the SOL by orbit loss ions for case 50 401 with 75 V/mm for background ions P_{i-i} and neutrals P_{i-n}.

mental values of peak ion heat flux q_i^{peak}, taking account of the uncertainties in TC/LP measurements and in the estimates of the radial electric field in the SOL (up to twice $3T_{e,t}/\lambda_q^{int}$ listed in Table 1). The experimental differences in q_i^{peak} between the natural density H-modes (50 401, 50 421) and fuelled H-mode (50 404) and L-mode (50 414) shots is clearly captured by ASCOT simulations. Due to the lower $E_{r,SOL}$ in the latter cases, ASCOT predicts quite small, and fairly symmetrical IOL heat loads, $q_{IOL}^{peak} < 2$ MW/m^2. In the former case, with $E_{r,SOL}$ in the range 30–60 V/mm, ASCOT underestimates the observed q_i^{peak} values by ~30% on the outer target, while matching the data quite well at the inner target. In other words, the observed in:out asymmetry in unfuelled H-modes can be explained in terms of IOL dependence on the SOL radial electric field.

Comparison of the simulated and measured integral power widths, λ_{IOL}^{int} vs. λ_{TC}^{int}, is only meaningful under conditions where ions dominate the target heat load, i.e. for shots 50 401 and 50 421. The contribution of the electron profile can be removed from the TC measured widths to estimate the ion power width, using the following expression

$$\lambda_{TC} \sim (q_i/q_{tot}) * \lambda_i + (q_e/q_{tot}) * \lambda_e. \quad (5)$$

Applying (5) to 50 401 and 50 421 and assuming an L-mode value of 7 mm-omp for λ_e, one obtains λ_i^{int} of 2.0 and 1.8 mm-omp, respectively (cf. λ_{TC}^{int} of 4.0 and 3.4 mm-omp). The actual ion power width is bounded by the above λ_i and λ_{TC}: 2.0–4.0 mm for 50 401, 1.8–3.4 mm for 50 421. Both results are relatively well matched by the ASCOT predictions of 2.6–3.0 mm-omp for 50 401 and 2.3–2.6 for 50 421. The range of simulated values corresponds to $E_{r,SOL}$ of 22–75 V/mm, implying that the outer λ_{IOL}^{int} is only weakly dependent on radial field in the SOL. The inner width, on the other hand, increases noticeably with $E_{r,SOL}$, from 6 to 10 mm-omp for the above cases. The origin of this broadening resides in the synergism between $\mathbf{E} \times \mathbf{B}$ and $\mathbf{B} \times \nabla \mathbf{B}$ drifts, which draw ions bound for the inner target away from the separatrix [3]. The above mechanism is of some importance in the interpretation of ELM broadening and will be investigated in a forthcoming study.

4.3. Interaction of orbit loss ions and SOL ions/atoms

As mentioned in Section 4.1, ASCOT records the location and properties of all collision events during the simulated ion's lifetime, both Coulomb collisions with background D^+ ions and charge-exchange (CX) collisions with D^0 atoms. By averaging over all ion trajectories (typically ~500 000 ions were used to assure good statistics) a 2-D distribution of energy and momentum transfer between the ions and the plasma/neutrals can be calculated. These will be discussed in turn.

2-D maps of energy deposited in the SOL by orbit loss ions for case 50 401 with $E_{r,SOL}$ of 75 V/mm is shown in Fig. 7(a) for background ions P_{i-i} and Fig. 7(b) for neutrals P_{i-n}. In both cases, the 2-D collision distribution closely reflects the background species density (inner divertor leg is always colder and denser, and detaches earlier than the outer leg). Specifically, the majority of i–n collisions occur in the immediate vicinity of the targets. Based on solid angle estimates, half of the newly created energetic neutrals would promptly deposit their energy on the targets. These neutrals may therefore increase the net heat load on the target.

Although not evident from Fig. 7, radial profile of IOL–SOL interaction is highest ~3 mm-omp away from the separatrix for both P_{i-i} and P_{i-n}. This value is insensitive to the radial field in the SOL. The integrated

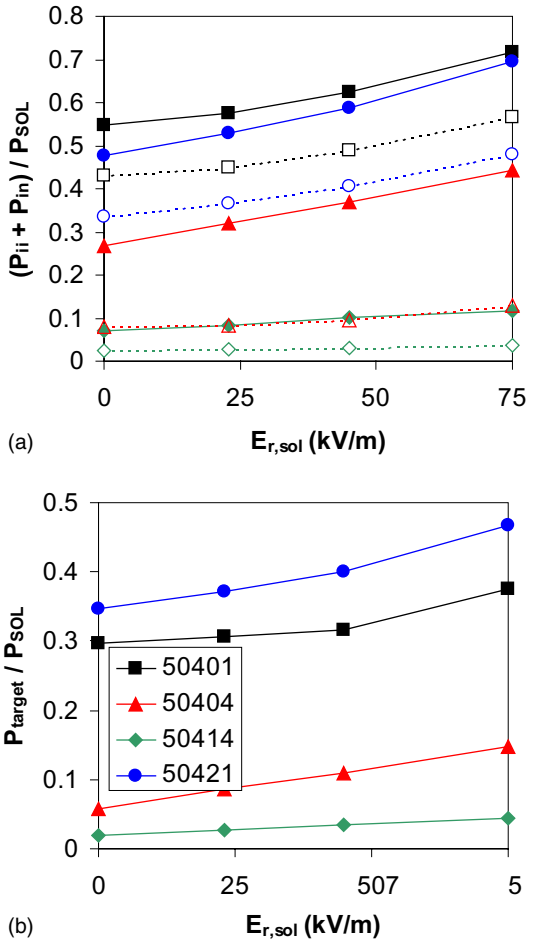

Fig. 8. (a) IOL power deposited in the SOL, $P_{ii} + P_{in}$, as a fraction of the measured power entering the SOL, $P_{SOL} = P_{NBI} - P_{rad}$ (solid symbols). Open symbols give the neutral only contribution, P_{in}/P_{SOL}; (b) IOL target power P_{target} normalized by P_{SOL}.

IOL powers deposited in the SOL, expressed as a fraction of the measured power entering the SOL, $P_{SOL} = P_{NBI} - P_{rad}$, are plotted in Fig. 8(a); for comparison, the target IOL power, normalized in the same way, is shown in Fig. 8(b). For unfuelled H-modes, i–n losses dominate. Additional fueling reduces the pedestal and increases i–i collisions in the SOL. The SOL stopping factor for IOL can be defined as the ratio of the net IOL power to the SOL, $P_{ii} + P_{in}$, and the total IOL power, $P_{IOL} = P_{target} + P_{ii} + P_{in}$ (since $P_{ie} \ll P_{ii}$ the electron contribution is left out of both expressions); this factor ~0.6 in unfuelled H-mode and ~0.8 in fuelled H- and L-mode. Comparable values can be inferred from a simulation with $n_e = n_i = n_n = 0$ in the SOL (50 401, 75 V/mm), where the target power was found to increase by 40% at the outer target and 150% at the inner target. This gives SOL stopping factors of 0.3 and 0.6 at the outer and inner target respectively. The contribution of IOL to the SOL power balance can be characterized by the ratio P_{IOL}/P_{SOL}, which is roughly unity for unfuelled H-modes, but only 0.3 in fuelled H-mode and 0.1 in L-mode. This result can be interpreted as pointing to neo-classical ion conduction in the ETB as being the primary mode of transport of energy into the SOL plasma. In the absence of the ETB (L-mode) or with the reduction of the pedestal (fuelled H-mode) neo-classical conduction is overtaken by growing turbulent transport and IOL becomes less and less significant in the SOL energy balance.

Similarly, 2-D maps of momentum deposited in the SOL by orbit loss ions for the same case is shown in Fig. 9(a) for background ions F_{i-i} and Fig. 9(b) for neutrals F_{i-n}. It is immediately clear that aside from the outer divertor leg, the entire SOL experiences a force directed anti-clockwise, towards the inner target. This force is in the opposite direction to the $E_r \times B_t$ drift which drives the ions to the outer target. Its direction is primarily determined by the SOL asymmetry (n_i, n_n, T_i) and may be understood as follows: ions heading to the outer target experience fewer collisions with the background ion/atoms than those bound for the inner target. This generates a net torque towards the inner target on both the plasma and neutrals. As with the energy, momentum deposition in the SOL peaks ~3–5 mm-omp away from the separatrix, the distance increasing with $E_{r,SOL}$. The integrated forces on ions and atoms are shown in

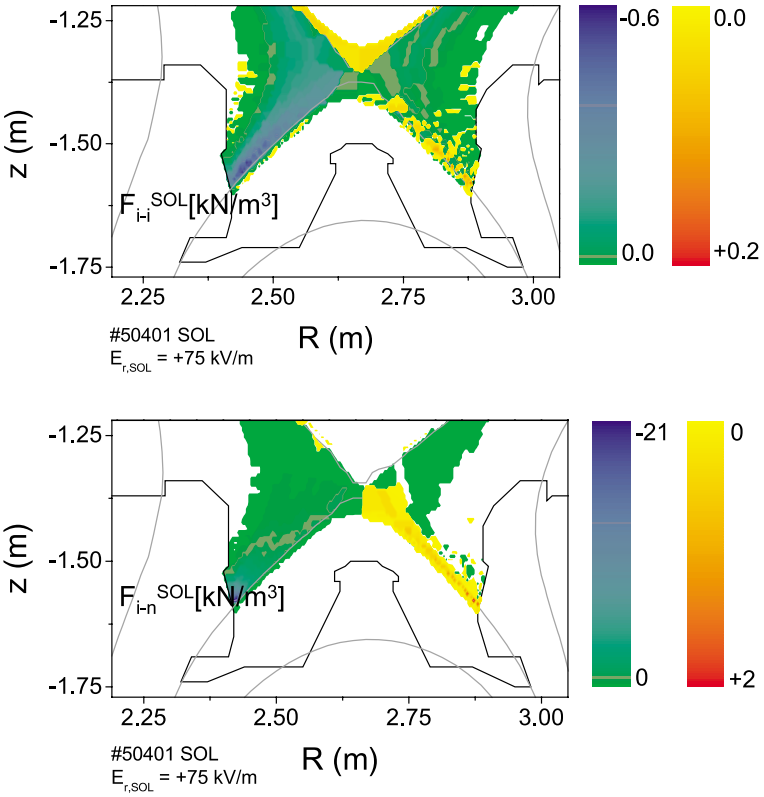

Fig. 9. Poloidal distribution of parallel momentum densities created in the SOL by orbit loss ions for case 50 401 with 75 V/mm for background ions F_{i-i} and neutrals F_{i-n}. Positive force points towards the outer target, negative toward the inner target.

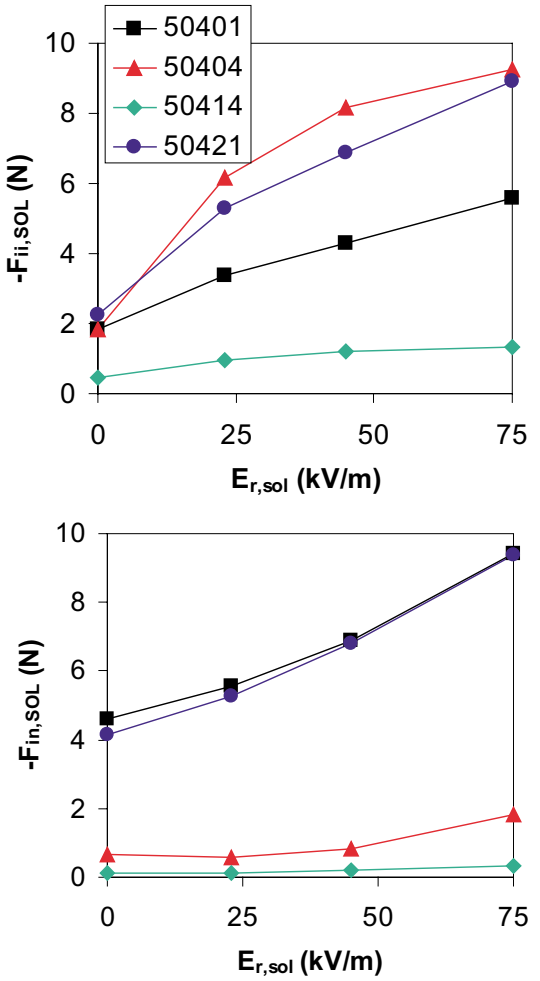

Fig. 10. IOL momentum deposited into SOL ions, F_{ii}, and neutrals, F_{in}.

Fig. 10. There is a strong increase in both F_{i-i} and F_{i-n} with $E_{r,SOL}$, with up to 10 N of force on ions and atoms in the SOL. Theses forces are smallest in the L-mode case, and largest in the high power H-modes. As with energy, additional fuelling increases the force on ions and reduces the force on atoms. First attempts to reconverge the plasma fluid solutions with the above momentum sources [15], indicate only a small increase in the SOL flow towards the inner target ($\Delta M_{SOL} < 0.1$). Hence, it is unlikely that IOL is the primary cause of the observed SOL flows which are typically much stronger, $M_{SOL} \sim 0.5$.

5. Conclusions

Recent JET results show an inverse power dependence of the SOL power width (profile peaking) in H-mode plasmas in contrast to the ITER-99 database. Numerical simulations support the hypothesis that IOL is responsible for this effect. The simulated IOL deposited power profiles for four JET discharges agree quite well (q^{peak}, λ^{int}) with the inferred (TC/LP) ion power profiles on both the inner and outer targets. Neo-classical ion transport appears sufficient to explain radial transport of power to the SOL in high power H-mode, but not in L-mode or fuelled H-mode. IOL couples momentum to the SOL ions which although in the same direction as the observed SOL flows are too small to be a primary cause of this flow.

In the future, IOL in ITER will be simulated. First simulations (plasma background from OSM2/EIRENE, pedestal width of 5 cm, $E_{r,SOL} = +150$ V/mm) indicate peak heat loads of $\sim$2 MW/m^2 at the outer target. This value should be reduce by the inclusion of neutrals, but is sufficiently high to merit more detailed ITER simulations.

Acknowledgements

This work was conducted under European Fusion Development Agreement and was partly funded by EURATOM and the UK Department of Trade and Industry. The authors would like to thank A. Kukushkin for providing them with an ITER background plasma.

References

[1] G.F. Matthews et al., J. Nucl. Mater. 290–293 (2001) 668.
[2] V. Riccardo et al., Plasma Phys. Control. Fus. 43 (2001) 881.
[3] W. Fundamenski, Plasma Phys. Control. Fus. 44 (2002) 761.
[4] W. Fundamenski, J. Nucl. Mater. 290–293 (2001) 593.
[5] R.D. Monk, Langmuir Probe Measurements in the Divertor Plasma of the JET tokamak, PhD Thesis, Imperial College, London, 1996.
[6] ITER database, many authors, Nucl. Fus. 39 (1999) 2423.
[7] R. Pitts et al., these Proceedings.
[8] W. Fundamenski et al., Phys. Rev. Lett., submitted for publication.
[9] J. Connor et al., Nucl. Fus. 39 (1999) 169.
[10] R. Simonini et al., Control Plasma Phys. 34 (1994) 347.
[11] W. Fundamenski, Tokamak Edge Plasma Modelling Using an Improved Onion-Skin Method, PhD thesis, U.Toronto, 1999.
[12] D. Reiter, J. Nucl. Mater. 196–198 (1992) 80.
[13] J.A. Heikkinen, Phys. Plasma. 8 (2001) 2824.
[14] P.C. Stangeby, The Plasma Boundary of Magnetic Fusion Devices, IoP, 2000.
[15] G.F. Matthews et al., these Proceedings.